Aeolian Research 57 (2022) 100813

Contents lists available at ScienceDirect

Aeolian Research

journal homepage: www.elsevier.com/locate/aeolia

Near-surface structure of a large linear dune and an associated crossing dune of the northern Namib Sand Sea from Ground Penetrating Radar: Implications for the history of large linear dunes on Earth and Titan

Clayton K. Chandler [a], Jani Radebaugh [a,*], John H. McBride [a], Thomas H. Morris [a], Clement Narteau [b], Karl Arnold [a,c], Ralph D. Lorenz [d], Jason W. Barnes [e], Alex Hayes [f], Sébastien Rodriguez [b], Tammy Rittenour [g]

[a] Department of Geological Sciences, Brigham Young University, S-389 ESC, Provo, UT 84602, USA
[b] Institut de Physique du Globe de Paris, 75005 Paris, France
[c] Occidental Petroleum, Houston, TX, USA
[d] Johns Hopkins University Applied Physics Laboratory, Laurel, MD 20723, USA
[e] Department of Physics, University of Idaho, Moscow, ID 83844, USA
[f] Department of Astronomy, Cornell University, Ithaca, NY 14853, USA
[g] Department of Geology, Utah State University, USA

ARTICLE INFO

Keywords:
Namib
Namib Sand Sea
Linear dunes
Superimposed dunes
GPR
Process sedimentology
Titan
Dunes
Sand seas

ABSTRACT

We imaged the near-surface sedimentary structures of a large linear dune, flanking dune forms and an associated crossing linear dune never before studied in the northern Namib Sand Sea using 200-MHz Ground-Penetrating Radar (GPR). The dry, uniform sandy conditions and wavelength used allowed for highly detailed observations of sedimentary structures to depths of ~ 12 m across a >1km lateral scan. Sedimentary features observed in the main linear dune include scouring and abrupt changes in strata such as trough cross stratification (TCS), onlap, downlap, truncation and avalanche-related bedding, all a result of complex sand transport conditions. Different phases of deposition have produced an opposed succession of strata on each side of the dune. These successions alternate 2-dimensional (2D), or bedform instability mode features with 3-dimensional (3D), or fingering mode features, separated by a clear process boundary. These alternating successions reflect a change in the dominant wind environment in the recent past. The changing winds may feed into the building and overall stability of this dune field and may be a model for conditions in other large linear/longitudinal dune fields. The subsurface structure of an oblique crossing linear dune demonstrates sand transport generally down the dune long axis in the direction predicted from modern, ERA-Interim model as well as paleoclimate model winds. This suggests relatively long-term stability of this intermediate-sized landform and the potential long-term coexistence of large dunes and secondary forms. These studies have implications for the extensive sand seas of Titan, where lack of large secondary forms may indicate a simple wind regime over long time periods.

Introduction

Large, linear dunes are a dominant landform in Earth's long-term, stable desert regions (Wilson, 1973; Lancaster, 1982). These landforms grow where sand is available to move and collect into features that are characterized by being highly parallel and having great lengths compared to widths (Lancaster, 1982; Lancaster, 1995). They fill regions termed sand seas, with stabilized forms in the Australian and South African deserts, among other regions, and with the largest and most active versions currently in the Saharan, Namibian and Arabian Deserts (Fryberger and Goudie, 1981; Wilson, 1973; McKee, 1979; Lancaster, 1989). These forms reach 1–2 km wide, 1–4 km in spacing, up to 200 m in height, and can be > 100 km long (Lancaster, 1982; Lancaster, 1995) and appear to have reached their maximum size based on sand availability and the thickness of the atmospheric boundary layer (Wilson, 1973; Andreotti et al., 2009). Their morphology is that of a single, long crestline, with slip faces that alternate from one side to the other, and an associated, broad, low-angle plinth down to the base (Lancaster, 1995).

* Corresponding author.
E-mail address: janirad@byu.edu (J. Radebaugh).

https://doi.org/10.1016/j.aeolia.2022.100813
Received 3 July 2018; Received in revised form 13 June 2022; Accepted 15 June 2022

The crestline can be sinuous, often with crescentic forms superimposed and having increasing complexity in various regions (Holm, 1960; Lancaster, 1982; Warren, 1988; Livingstone et al., 2007). They can also have multiple, parallel ridges on a single, broad plinth (Mainguet and Callot, 1978; Lancaster, 1982). Nearly all large linear dunes have smaller associated flanking features that are transverse, crescentic or linear in shape. On human timescales, the margins of large linear dunes appear to be stationary even though they exhibit a high level of activity on their crests and flanks (Tsoar, 1983; Livingstone, 1989; 1993; 2003).

The long-term processes that build large linear dunes are the subject of much modern research. When discussed in conjunction with wind and sand transport directions, these dunes have been termed "longitudinal" (Wilson, 1972; Cooke and Warren, 1973), one interpretation of that being that combined factors, including multi-directional winds, result in sand transport occurring more or less parallel to the crest (Fryberger, 1979; Tsoar, 1983; Courrech du Pont et al., 2014). Models and lab experiments have shown that two dominant winds with an obtuse angle (Rubin and Ikeda, 1990; Reffet et al., 2010) or a major, off-axis wind with a secondary wind (Courrech du Pont et al., 2014; Courrech du Pont, 2015) are sufficient to form and maintain longitudinal dunes. But knowledge of exactly how past and present winds have shaped the main dune as well as the flanking dune forms, and how well the dune preserves any changes that have occurred over time (Munyikwa, 2005; Singhvi and Porat, 2008), is still elusive. Thus, going back in time, through analyzing dune layering in the subsurface using Ground Penetrating RADAR (GPR) and pairing these studies with age dating from Optically Stimulated Luminescence (OSL), has revealed more details about the histories of linear/longitudinal dune sediment transport than surface field studies alone (Tsoar, 1982; Bristow et al., 2000; Bristow et al., 2005; Bristow et al., 2007). This study thus not only develops the utility of the Namib Sand Sea linear dunes as a proxy for wind direction during the Quaternary, but provides a morphological analogue for a major landform found on Titan.

This paper aims to shed further light into the evolution of large linear dunes, and how this relates to wind patterns during the Quaternary. Large linear dunes comprise the greatest proportion of dunes in Earth's big deserts worldwide (Lancaster, 1989). Similarly, large linear dunes morphologically analogous to those on Earth cover ~ 15% of the surface of Saturn's moon Titan (Lorenz et al., 2006; Rodriguez et al., 2014; Arnold, 2014). We use new, high-resolution, two-dimensional (2D) GPR data to investigate near-surface (~12 m deep) deposits of a large linear dune and a smaller, associated linear crossing dune in the northern Namib Sand Sea that reveal past and present sedimentation patterns.

Geologic setting and study area

The Namib Sand Sea, located on the western coast of southern Africa (Fig. 1), overlies the sandstone deposits of the Tertiary (pre-Miocene to Quaternary) Tsondab Sandstone (Kocurek et al., 1999) and the Namib platform (McKee, 1982), an unconformity surface developed on late Precambrian bedrock (Kocurek et al., 1999). The majority of the sand in the Namib is from the Orange River, which is near the southern edge of the sand sea (Vermeesch et al., 2010), and is mainly well-sorted and well-rounded quartz.

Similar to other large, linear dunes, the dunes of the Namib Sand Sea can be up to 200 m tall, hundreds of kilometers long, 2 or more kilometers wide and spaced up to 4 km apart (Lancaster, 1995). The large linear dunes of the Namib are regionally straight for tens to hundreds of kilometers, but on a local scale have a significant amount of crestline sinuosity (Figs. 1 and 2). Dunes of the Namib have been subdivided into type and have been given context with respect to regional winds by Livingstone et al. (2010).

Previous studies in the northern Namib Sand Sea have analyzed the relative movement and rate of change of dunes. Bristow et al. (2000) found through a deep penetrating GPR survey that lateral transport occurs at the end of a linear dune in the northern Namib Sand Sea

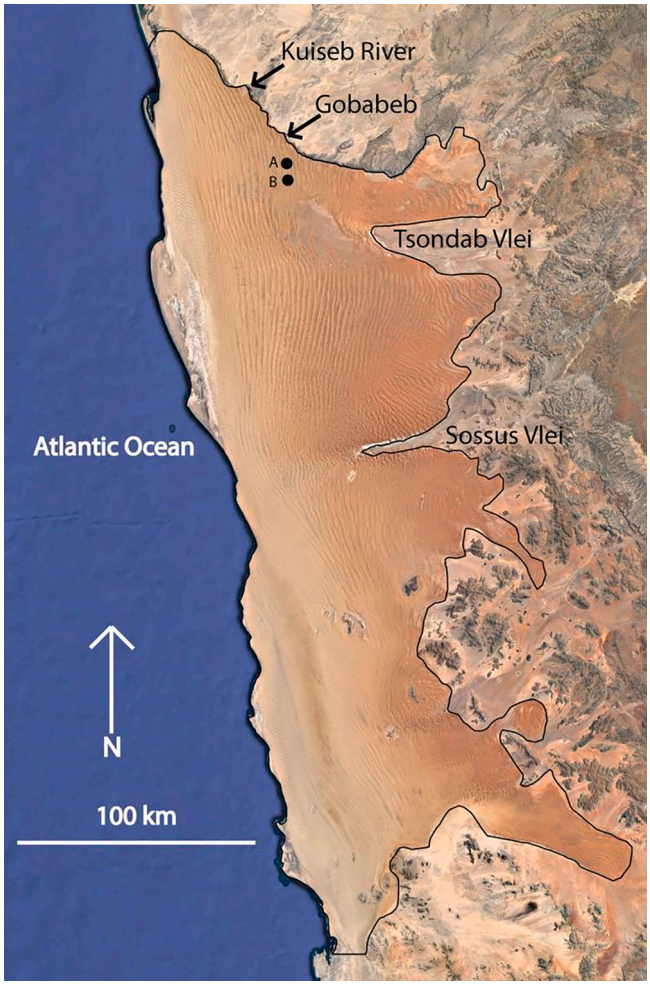

Fig. 1. The Namib Sand Sea (black outline based on presence of dunes), located on the southern Atlantic coast of Africa, from 27 to 23° S and 14.5 to 16.5° E. Large linear dunes are visible trending N-S throughout the central portion of the sand sea. The vleis are entrants of ephemeral river channels draining from the eastern highlands. Black dots labeled A and B are locations of study sites. Base image from Google Earth courtesy of Landsat.

(Fig. 2). Bristow et al. (2005), using internal layering measured by GPR and dates from OSL, found that part of a dune located ~ 5 km south of Gobabeb had moved an average of 0.12 m/year since ~ 432 CE (Fig. 2). Studies of the core of a dune revealed deep internal overturn ages of 5700 years (Fig. 2; Bristow et al., 2007). Livingstone (1989, 1993, and Livingstone, 2003) periodically monitored and surveyed a dune for twenty-one years (1980 to 2001) finding that, though the crest was active, there was no discernable movement on the dune margins.

This study focuses on two sites within the northeastern part of the Namib Sand Sea, an area characterized by complex linear dunes (Lancaster, 1989), often over 100 m tall, trending approximately north–south (Fig. 2). The first site (Site A) is a section of large linear dune ~ 12 km south of Gobabeb Field Station where the dune is ~ 120 m tall and 1200 m wide (Fig. 2). This dune's shape and size are characteristic of the large linear dunes throughout the center of the Namib Sand Sea (Fig. 3a) and it is fairly centrally located in the dune field where edge effects, which may act to bias studies, could be avoided. The dune crestline is highly sinuous and divides into multiple crestlines to the north and south, but it has a single and relatively straight crestline and loose sands near the study site (Fig. 4a). The second field site (Site B) is farther to the south and is a region where a smaller linear dune extends northeast from a large linear dune (Fig. 3c and d; Lorenz and Radebaugh, 2016).

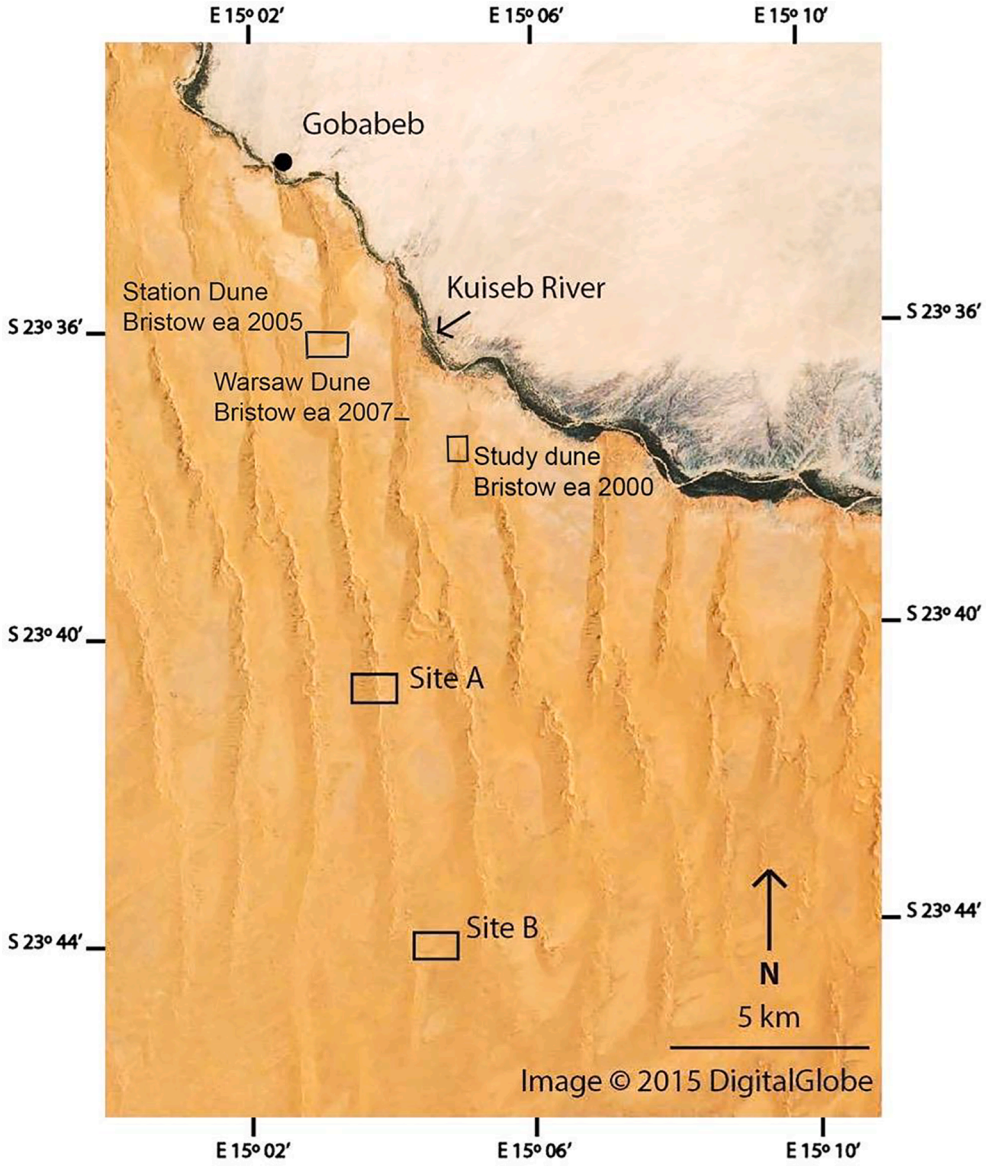

Fig. 2. The northern Namib Sand Sea and location of our field sites. Site A is the large dune site (see Fig. 4 for greater detail). Site B is the crossing dune site (see Fig. 5 for greater detail). Study areas for previous work are also indicated. Base image from Google Earth.

The eastern margin of the study dune, in its lower reaches, displays a gentle, uneven slope of shallow grade of 6° −7° (Fig. 4a, b right side of transect). The eastern slip face of the crest is ~ 25° from ~ 90 m until the crest. The west side of the dune is also at the angle of repose from the crest to ~ 15 m away, then more gradually slopes down to the interdune surface (Fig. 4a, b left side of transect). In much of the sand sea, and in our study area, these primary linear dunes have smaller, superimposed dunes on their flanks (Fig. 4a).

The second field study site (Site B) is about 7 km south of our large dune and located where a small linear crossing dune extends diagonally in the ENE direction away from a large linear dune (Fig. 3c). These unusual forms have an orientation consistent with each other over several tens of kilometers across the sand sea (Fig. 5), at an azimuth of ~ 65° from the primary dune long axis. The crossing dunes reach across the interdune, approaching the adjacent large linear dune (Fig. 3d). The crossing dune is linear in form and asymmetrical in cross section, with the northwest side steeper than the southeast side, and has a sinuous and discontinuous crest (Fig. 5). The study crossing dune is ~ 10 m tall, ranges from 100 to 200 m wide (it is wider at what is postulated to be the initiation region, at the southwest), and is 1.3 km long.

This crossing dune is representative of a number of dunes with similar characteristics in size, shape and morphological relationship to the large linear dunes in the region (Fig. 3c), and some similar forms in the south have been discussed (Bubenzer et al., 2007; Stone et al., 2015). The form may be part of a morphological continuum between the short transverse forms called “raked dunes” by Dong et al. (2010) and the fully two-dimensional “aklé” pattern seen on Mars, or the “trellis” forms in the Arabian desert (see Lorenz and Zimbleman, 2014, chapters 2.5 and 2.6 - e.g. figure 2.5.27). In particular, the crossing dune in this study does not quite fully span the space between the dominant linear dunes, whereas in the eastern part of the Rub Al Khali in the United Arab Emirates (Lorenz and Zimbleman, 2014, figure 2.6.14) the crossing dunes completely bridge the gap between the primary linears to form a trellis. The near-rectilinear two-dimensional pattern among predominantly linear forms is also seen in locations on Titan (e.g. Lorenz and Zimbleman, 2014, figure 2.5.15; Ewing et al., 2015).

The interdune regions of both study areas are characterized by having different materials and properties than the dune regions (Fig. 6a, b). Sands are present low on the dunes and into the interdunes as gradually terminating plinths that give way to interdune materials. The

Fig. 3. (a) The size and complexity of the Namib large linear dunes as viewed from the large study dune, looking W; small figures at lower left are people. (b) Method of our GPR traverse of the main dune. (c). View from the air, to the SW, of crossing dunes extending from large linear dunes near the study area. (d) Kitecam image looking to the SW of the crossing dune joining the main dune at image top. Pics a, c, from Jani Radebaugh, b from Jason Barnes, d from Ralph Lorenz.

interdune surface is mostly silty with some coarse sand and sparsely distributed, rounded quartz cobbles, some translucent, up to 4 cm in size (Fig. 6c). The surface silts are generally light tan in color, and some regions of deflation have a layer of coarse sand covering the silt. At depth, the soil is silty and deep red in color (Fig. 6d), probably because of oxidation of the true soils. The dune sands, on the other hand, are a rust/buff red, indicating the difference in origin and evolution of the interdunes and dunes. There is also a difference in distribution of vegetation – near the crests of the large and crossing linear dunes, where dunes are most active, vegetation is absent. On the plinths, there are grasses and shrubs spaced every 0.5–3 m (Fig. 6a, b), but there is no vegetation found in the interdunes. Perhaps this is because the sandy plinths allow for infiltration of water from episodic rainfall (a high amount of precipitation fell during the previous rainy season; Theo Wassenaar, Pers. Comm.) or daily fog noted to be present in the Namib, whereas the interdune remains relatively dry at depth, and the cohesive clays would preclude infiltration (Fig. 6d).

Ground penetrating radar study

Methods

GPR instrumentation and processing were chosen to balance obtaining a high depth of penetration with achieving a high spatial resolution. During our field campaign on 8–9 August 2013, two GPR transects were collected on the primary linear dune, from the eastern plinth to the crest and from the crest down to the edge of the western plinth (Fig. 3b, 4a). GPR data were also collected on a dune farther south (site B of Figs. 2 and 5). These two datasets were collected using a Geophysical Survey Systems Inc. (GSSI) antenna with a central frequency of 200 MHz. Data were acquired in continuous mode with a trace every 0.06 m. Traces were collected over 200 ns and sampled every 0.20 ns. Topography was obtained using a Trimble GeoExplorer 6000 Series handheld Differential Global Positioning System (GPS) instrument corrected using the Windhoek reference station and coupled to the GPR antenna throughout the survey.

The data were processed with a method that included removing the direct arrival, exponential gain balancing, trace mixing, 2D phase shift migration, time to depth conversion, and topographic correction. Depth conversion was performed using a velocity of 0.122 m/ns (yielding a vertical resolution of 15 cm based on the Rayleigh criterion) calculated from a dielectric constant (ε) of 6 which assumes a mixture of quartz sand and air (23% porosity) with minor amounts of organic matter, iron oxide and moisture. This velocity is consistent with what is often used for dry sand (0.15 m/ns based on common midpoint surveys in the Namib from Bristow 2007) and it produced the best migration and flattened the interdune surface as we expected.

Ground Penetrating Radar (GPR) responds to changes in the electrical properties of the ground measured as the dielectric constant. In the case of dune sand, we assume that GPR reflectivity is caused by large-scale sedimentary structures (Bristow, 2009) that contain small variations in porosity of the sand, typically caused by a grain size change resulting from wind differences (Topp et al., 1980; Huggenberger, 1993). In most cases we assume that these variations in porosity are equivalent to sedimentary structures or sequence boundaries (Gawthorpe et al., 1993; Van Dam and Schlager, 2000; Bristow, 2009). Enhanced water content can also change the magnetic permeability and affect the radar return (Van Dam and Schlager, 2000).

Main dune GPR survey results

Our 200 MHz GPR survey yielded overall penetration depths of up to ~ 12 m ($\varepsilon = 6$), which indicates the sand was likely very dry and optimal for signal transmission. We obtained a GPR profile for the entire dune across the trace indicated in Fig. 4a (Supp Fig. S3).

We focus these analyses on the GPR data obtained on the flanks of the dune on both sides, adjacent to the slip faces (Fig. 7c for locations). On the western flank of the primary dune (Fig. 7a) we see near-surface (to a

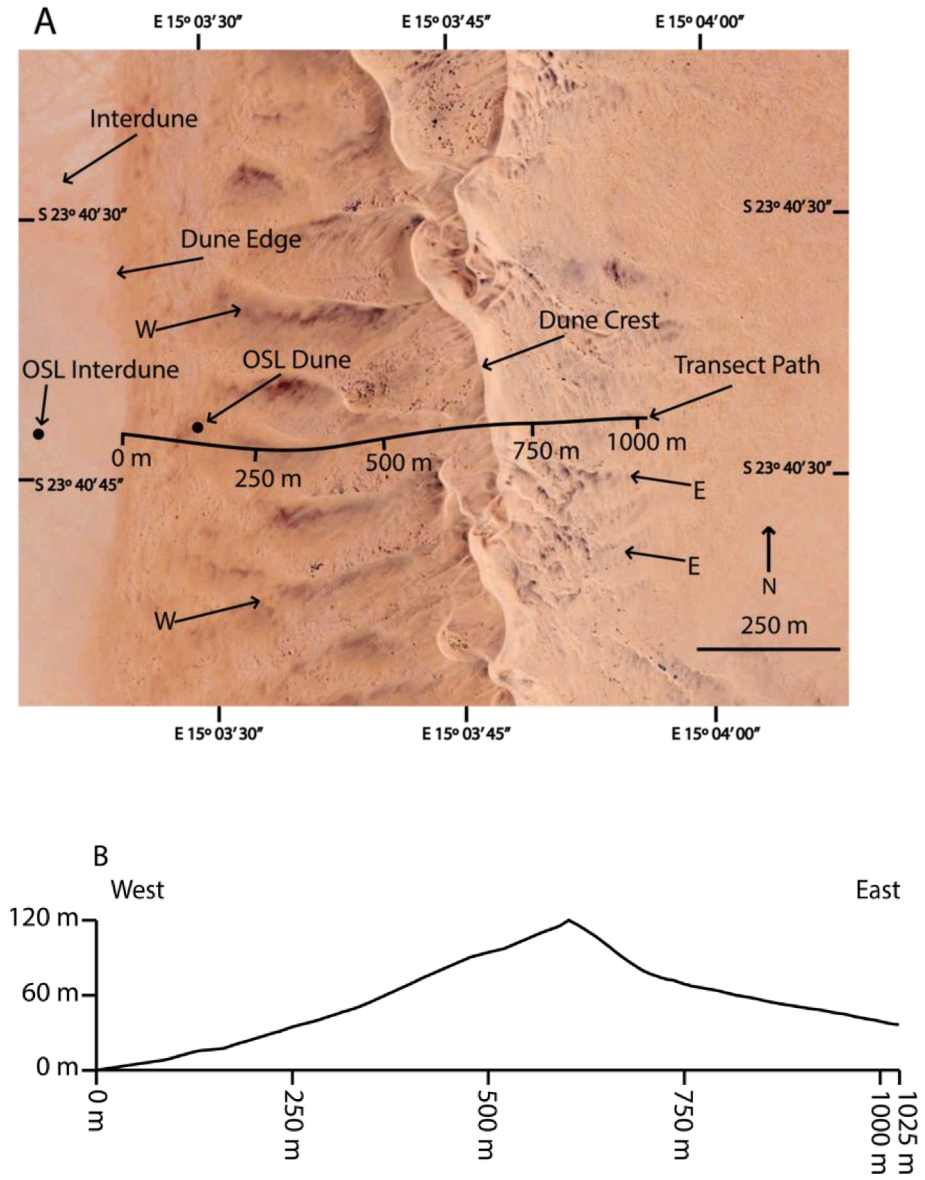

Fig. 4. (a) Site A in Fig. 2. Black line (labeled transect path) is location of the study GPR transect, the elevation profile of which is displayed in (b). Arrows A and B are pointing to superimposed dunes on the west (W) and east (E) sides of the primary linear dune. Arrows indicate where OSL (Optically Stimulated Luminescence) age dating samples were obtained from the plinth of the dune and the interdune. Base image from Google Earth and Digital Globe.

depth varying from 1 to ~ 3 m) reflections that are nearly parallel with the surface of the dune (Radar Facies 2 in Fig. 7a). These reflections can often be followed for more than 100 m and terminate in gentle onlap (younger, or higher, strata extending across older, or lower, erosional surfaces), downlap (younger, or higher, steeply-dipping strata terminating against older, or lower, more gently sloping strata) or low angle truncation (termination of strata) by the dune surface. Below these shallow reflections exists a definitive boundary that separates two radar facies; this boundary is a stratigraphic change herein termed the superposition surface, a bounding surface similar to that observed on the west side of another dune by Bristow et al. (2007; Fig. 7a). A bounding surface generally reflects a change in depositional style, particle size or composition (Kocurek, 1981; Kocurek and Havholm, 1993). On the western flank below the superposition surface (Fig. 7a, Radar Facies 1, from the base of the surface reflections at 1 to 3 m to the penetration limit at ~ 12 m) we see much shorter reflections (rarely more than 20 m long) at much higher angles that terminate in sharp truncations, high angle downlap, or onlap (rare). Packages of reflections in this part of the data often truncate other packages of reflections. Several bowl-shaped packages of reflections can be seen in this part of the data (Fig. 7a, around 380 m and 350 m on the horizontal axis). The deeper strata found in Radar Facies 1 are characterized by being complex, in contrast to the simple near-surface strata in Radar Facies 2, seen clearly in the zoomed Fig. 8a. These relationships indicate the bounding surface is either second-order, in which migration of superimposed dunes migrate over the larger dune, or third-order, which is a reactivation surface that demonstrates stages in the advancement of individual dunes (Havholm and Kocurek, 1994).

Low on the eastern flank of the primary dune (Fig. 7b) we see near the surface (to a depth varying from 1 to ~ 3 m, Radar Facies 4) reflections that are wavy, nonparallel, and in some areas discontinuous. These reflections can usually only be followed for a few meters and terminate in onlap, downlap or low-to-moderate angle truncation by the dune surface or subsurface strata (Fig. 7b, 8b). In the deeper part of the data (Fig. 7b, Radar Facies 3, from the base of surface reflections at 1 to 3 m to the penetration limit at ~ 12 m) on the eastern flank of the primary dune, we see much longer reflections (often 50 m or more) that terminate in gentle-to-moderate truncations, downlap, or onlap. Many

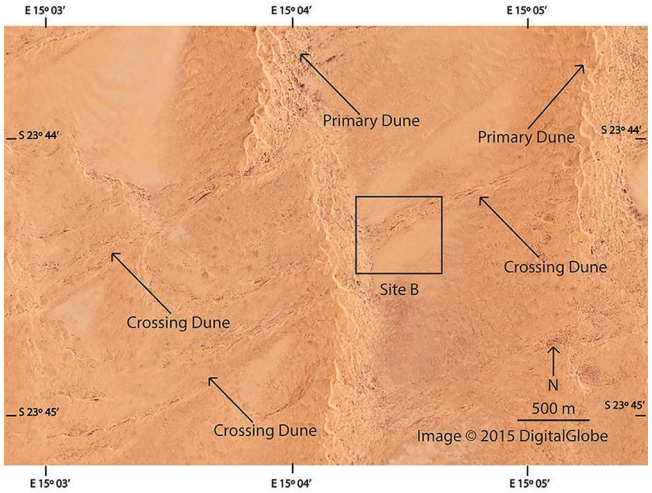

Fig. 5. Location of crossing dune study area and GPR collection site (Site B). The relationship between the primary large linear and crossing dunes are shown as well as the orientations of the crossing dunes in this area. Base image from Google Earth.

of these features were also seen by Bristow et al. (2005). On the east side, the deeper, Radar Facies 3 strata are simple, while the near-surface, Radar Facies 4 strata are relatively complex, as seen in the zoomed Fig. 8b. We note that the process boundary here is not as clearly delineated as on the west side.

These observations reveal that there is a reversal in the stratigraphic patterns seen on either side of the dune. On the west side, there are simple stratigraphic patterns near the surface and complex patterns at depth, while on the east side the patterns are simple at depth and complex near the surface (Fig. 8a, b). Near the crest of the dune on both sides, but especially on the eastern side, which is the more recent slip face, crestline movement and avalanching dominates (Fig. 9). Long reflections are sub- parallel to the dune surface and terminate near the inflection point of the dune (where the slope of the dune decreases). Here, reflections with flank characteristics interfinger with the terminations of the reflections that originated near the crest (Fig. 9).

Crossing dune GPR results

We obtained data at the linear crossing dune field site farther south in the Namib, Site B (Figs. 2 and 5). On the crossing dune, the penetration depth was limited to 10 m or less. The data set includes six GPR lines (Fig. 10), one along the crest of the dune (strike line) and the rest crossing the dune at different points (dip lines). Along the strike line, there are packages of reflections bounded by downlap at the base and truncation at the top (Fig. 11a). These packages range in size from 1 to 5 m thick and 5 to 100 m or more long. The majority of these packages contain reflections that dip to the east end of the line (a few have negligible dip and some within 2 m of the surface parallel the surface and dip to the west; Fig. 11a).

Crossing the dune and along the dip lines, there are packages of reflections bounded by downlap on the base and truncation at the top (Fig. 11b). These packages range in size from 1 to 5 m thick and up to 45 m long. The majority of these packages contain reflections that dip to the north, with the notable exception of a single package on the south side of

Fig. 6. (a) Interdune (foreground) and dune (background) taken midway along our track to Site A, as viewed into the sun, to show the roughness as revealed by shadows of the interdune cobbles and difference in color based on illumination angle (dunes in a and b are similar actual colors). Note lack of vegetation on the interdune. (b) Interdune (foreground) and dune (background) illuminated from behind the photographer, to show the difference in color, related to composition, of the dune and interdune. (c). Interdune surface showing large, translucent quartz and other cobbles, some with ventifact (wind erosional) features, and coarse sands overlying silts. (d) Pit in the interdune shows fine-grained nature and presence of oxidized soils. All photographs are taken by Jani Radebaugh.

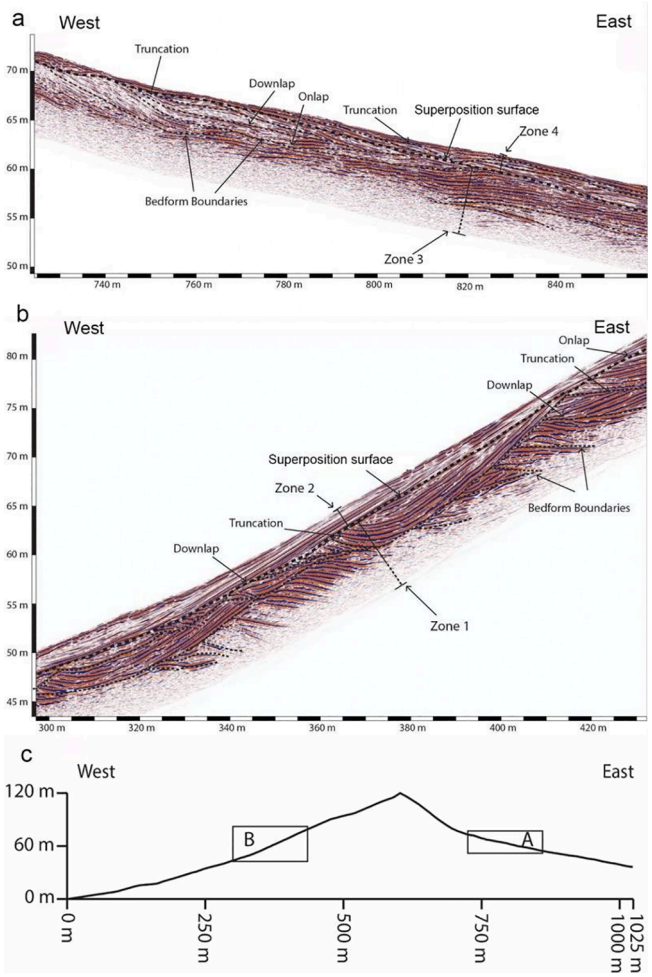

Fig. 7. (a) Excerpt of western side of the large linear dune GPR profile (site A of Figs. 1 and 2, transect shown in Fig. 3). (b) Excerpt of eastern side of the dune (does not go all the way to the crest). The bold dashed line indicates the location of the superposition surface, described in the text. Other dashed lines indicate divisions between strata. Labeled reflector termination types (onlap, truncation, downlap) were used to distinguish sedimentary packages. Radar Facies referred to in the figure discussed in text. (c) Dune profile with locations of GPR excerpts in (a), (b).

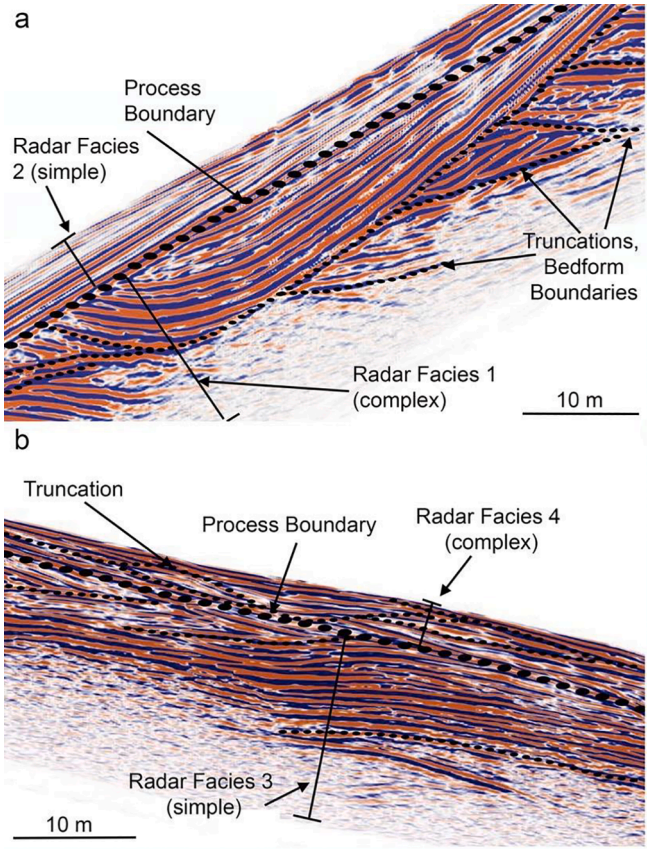

Fig. 8. (a) Zoom of western side of the large dune GPR profile. Note the bedform truncations and other complex patterns in the lower Radar Facies 1 as compared with the smooth, parallel strata in Radar Facies 2, separated by a clear superposition surface. (b) Zoom of eastern side of the large dune GPR profile. Note the complex patterns in the upper Radar Facies 4, while below the superposition surface in Radar Facies 3 the strata are relatively parallel and simple.

the peak of the dune that has reflections that dip to the south. The combined result of these transects reveals that the motion of the sediment is to the north-northeast, at some vector between the orientations of the two GPR lines.

OSL ages for dune and interdune sediments

We obtained Optically Stimulated Luminescence (OSL) age dates of three samples, one low on the western flank of the large linear dune and one nearby in the interdune of the large linear dune (locations in Fig. 4a). OSL dating measures when quartz grains were last exposed to sunlight, and sands here are dominated by quartz, in this area 75–80%, with feldspars and other lithics including basalt fragments and pyroxene (Garzanti et al., 2012), which prove to be magnetic. The particles are characterized by being rounded and polished, with iron oxide coatings (Fig. 12b; Garzanti et al., 2012). As described earlier, the interdune in our study area had a surface of sand and clay mixed with gravels of rounded, translucent quartz up to several cm in size (Fig. 12d). Below the surface of the interdune, in our sample pit, the material was deep red, sandy soil (Fig. 12c). Samples were collected by digging down to a depth of 0.5 m (interdune; Fig. 12c) and 0.7 m (dune; Fig. 12a), at which a sample canister (pipe) was pounded into the sand horizontally and extracted and carefully capped, retaining the sample and preventing sunlight exposure. Cohesion from clay content helped hold the interdune soils together. Samples were analyzed using single aliquot regenerative dose procedures for dating quartz sand (See Section S9.2, Murray and Wintle, 2000, 2003; Wintle and Murray, 2006).

Our luminescence data (Table 1 and 2) reveal a sediment exposure age at 0.7 m depth in the lower flanks of the west side of the primary dune of 110 ± 70 years (Namib 2 in Table 1). Samples previously obtained from a western Namib dune flank at 3.34 m depth revealed ages of 340 years (±20 years; Bristow et al., 2005), while samples recovered through drill cores from the base of a Namib linear dune were aged ~ 5700 years (Bristow et al., 2007). In contrast, a sample from an interdune west of the primary dune obtained at 0.6 m depth was dated at 51 ka ± 7.8 ka; (Namib Interdune 1 in Table 1). This reveals considerable overturn in the dune sands compared with the interdune, which appears to have been a stable surface throughout much of the late Pleistocene. For further comparison, a lower dune flank sample obtained in the Narabeb (in the Namib Sand Sea midway between Tsondab Vlei and the ocean) at 7 m depth records an age of 68.3 ± 5.7 ka and a remarkable 132.3 ± 15 ka near the dune base at 0.5 m depth (Stone et al., 2010). A dune in the southern part of the Namib Sand Sea at 2 m, 3 m and 4 m depth on the west side recorded ages of 15.6 ± 1.3 ka, 18.76 ± 2.08 ka and 18.56 ± 1.14 ka and another dune near the first at the same depths on the east side was 9.04 ± 0.76 ka, 8.79 ± 0.79 ka and 10.42 ± 0.66 ka (Bubenzer et al., 2007). Finally, we also obtained samples from 1 m below the floor of the sand-covered Roter Kamm impact crater, located

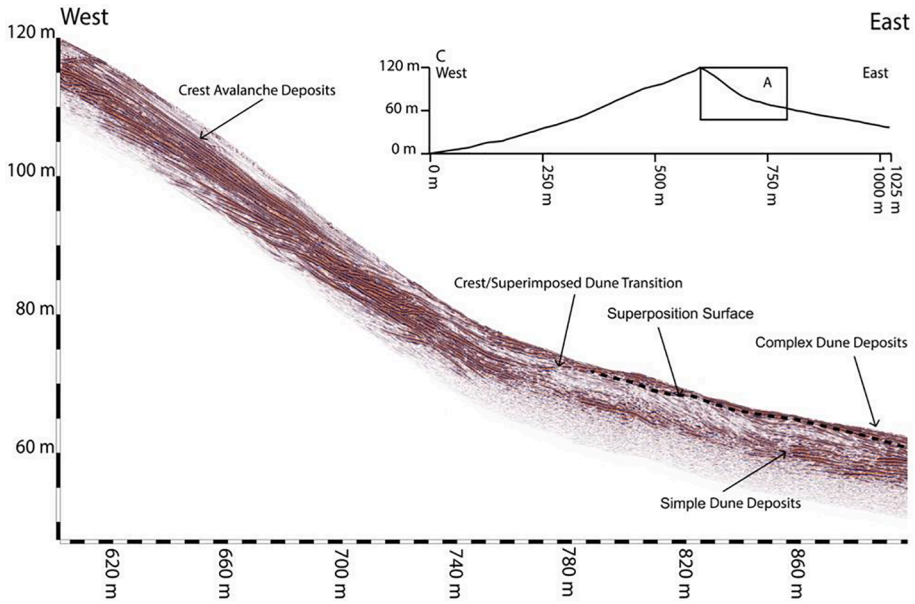

Fig. 9. GPR profile from the crest (far left) through the transition to the flank deposits (middle to right), revealing the differences in these deposits. Strata broadly parallel to the long slip face are the result of gravity-driven mass wasting. These transition to more complex flank deposits.

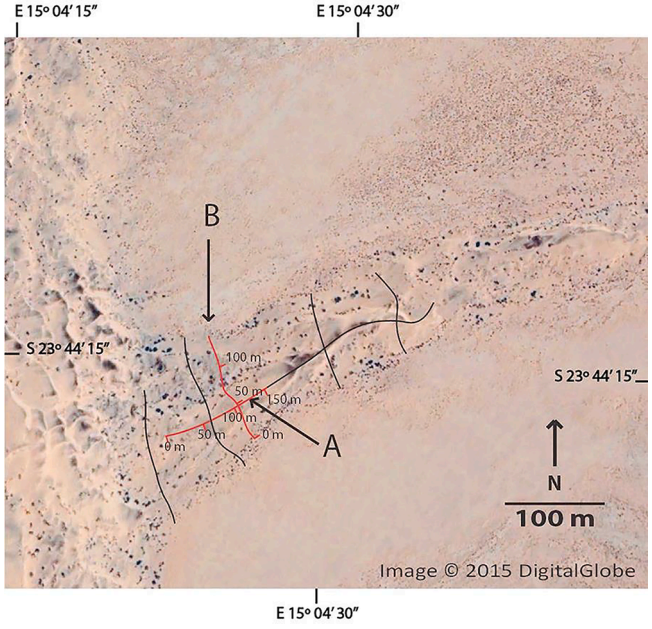

Fig. 10. Close up of crossing dune Site B. Red lines show locations of crossing dune GPR data in Fig. 11. Black lines show where other data were collected. Black dots in the image are bushes and other vegetation. Base image from Google Earth.

south of the Namib Sand Sea and 460 km south of our study dune and found them to be 43.7 ± 8.4 ka (Namibia Roter Kamm 1 in Table 1; Lorenz and Radebaugh, 2016). Such figures reveal that dune overturn is more common than interdune overturn in the Namib, and the depth of sampling within a dune is important; it is possible that deeper sampling within our dune of study would have yielded older ages (Table 2).

Discussion

Large linear dune GPR interpretation

The high resolution of our data down to ~ 12 m depth allowed detailed interpretations based on clear and well-known sedimentary relationships. We interpreted these data by grouping radar facies, or different reflectivity patterns, representing distinct depositional processes (e.g. Kocurek and Havholm, 1993). We identified five major depositional signatures across our dune transect that we describe below (Fig. 13).

Radar Facies 1 – The deeper part of the western flank of the large linear dune from 1 to 3 m deep down to our penetration depth at ~ 12 m encompasses this zone (Fig. 7a and 13). It is characterized by cross-cutting concave reflections, indicative of the processes of scouring and fill (Fig. 7a and 8b). These reflections can be interpreted as sedimentary structures consistent with trough cross-stratification (TCS), which in this case results from deposition by turbulent flow of wind (Bristow et al., 2000). Dunes formed by this kind of turbulent flow are three-dimensional (3D), meaning that variations in the dune are expressed in ×, y and z directions. In this location, we interpret the sedimentary patterns as being a result of the presence of secondary dunes with crests that were sinuous, potentially discontinuous, and with varying heights along the main dune. We interpret the TCS here to be deposits from 3D superimposed dunes on the flank of the primary linear dune. (Note that only a single GPR trace was obtained, and it was oriented along an E-W track, so strict 3D interpretations are not possible with this dataset.) We envision these dunes to be similar to those seen on the east side of the main study dune in Fig. 4a and in Fig. 14 in the area labeled "3D superimposed dunes," both in shape and in relationship to the primary dune.

Superimposed dunes have been noted in GPR data of lower resolution (i.e., using a lower-frequency antenna in order to obtain greater depths of penetration; Bristow et al., 2000; Bristow et al., 2007). Those studies noted TCS from superimposed dunes on their study dunes to depths of less than 10 m on a large linear dune at the northern margin of the sand sea (Bristow et al., 2000; Bristow et al., 2007). Given that our observations revealed slightly thicker TCS, it is possible these superimposed dune forms are slightly larger/deeper closer to the center of the sand sea.

Radar Facies 2 – This is the shallower part (from the dune surface down to 1 to 3 m) of the data on the western flank of the dune (Fig. 7a and 11). It is characterized by long reflections (up to 100 m or more) that are nearly parallel to the surface of the dune with gentle terminations (low angle downlap and low angle truncation). Our single GPR trace

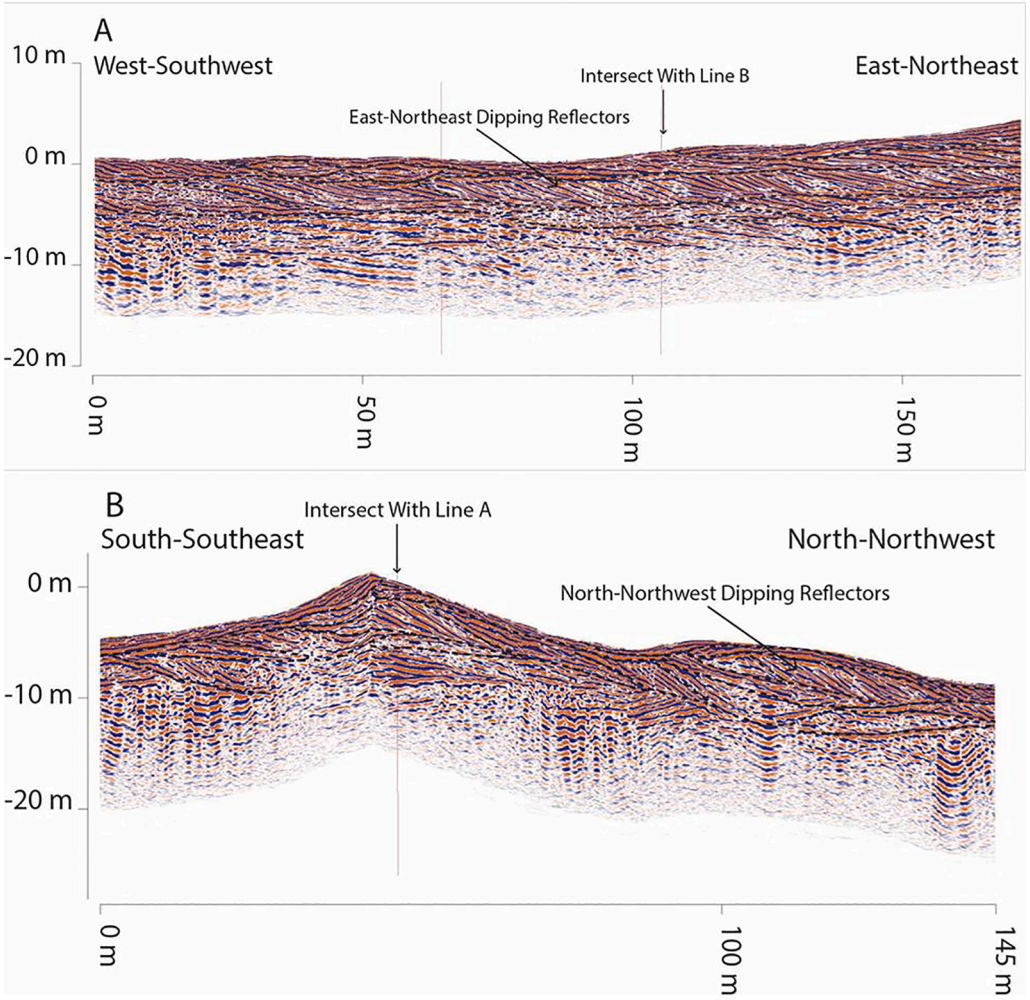

Fig. 11. (a) GPR trace collected down the crest of the linear crossing dune, red line "A" in Fig. 10. The apparent dip of the foresets is to the east-northeast. (b) GPR trace across the crossing dune, the red line "B" of Fig. 10. The dominant dip of the foresets is to the north-northwest; similar profiles were recorded for the other transects. The combination of these observations indicates that motion of the sand along this dune is to the north-northeast, about 45° off the dune axis.

sampled depositional features that are generally parallel to the surface. Duneforms on the surface on the west sides of the large dunes (Fig. 14 left side) are simple transverse dunes with sand transport generally to the north (from modern wind conditions). These dunes are two-dimensional (2D), meaning that variations in the dune typically involve movement along just a single direction and having a consistent height and wavelength. In this location we interpret the planar stratification to be the result of the GPR transecting deposits of simple 2D superimposed dunes on the flank of the primary dune parallel to the 2D dune long axis and perpendicular to the direction of flow. Because this is the surface layer on the west side, This deposit represents the current process occurring there, visible as E-W oriented simple transverse dunes with a northward sand transport direction (Fig. 14).

Radar Facies 3 – This facies is found in the deeper portion of the east side of the dune, from 1 to 3 m down to the penetration of the data at 12 m (Figs. 13 and 7b). It is characterized by long reflections (often more than 50 m) that cross-cut each other and terminate more gently than in the deeper portion of the dune on the other side, in Zone 1. This reflection pattern is consistent with 2D dune architecture with an added element of sinuosity. A gently sinuous wave front to northward-migrating 2D dunes, for example, might produce long, low-angle beds that cross-cut each other (Fig. 7b).

Radar Facies 4 – This facies is found on the eastern flank of the dune from the surface down to 3 m depth (Figs. 13 and 7b). It is characterized by short, (only a few meters) wavy, discontinuous reflections that cross-cut each other. The reflection terminations in this facies are at a greater angle to the adjacent strata than those found below, in Radar Facies 3, and are more consistent with TCS. In this location, we interpret the pattern to be the result of deposition by 3D dunes that, because of the smaller layer depth and lower cross bed angles, are less sinuous than those that are deposited in Radar Facies 1. Because this is the top layer on the east side, we assume this represents the process happening here currently, or the passage of 3D dunes along the flanks (Fig. 14). It should be noted from the transect line in Fig. 3 that this part of the transect was probably collected in the deflationary trough between two wave fronts and this zone would likely appear thicker if it were collected along the ridge of one of the superimposed dunes. It should also be noted that all of the deposits on the east side of the dune are more similar to each other than the deposits on the west side are to each other. However, on the east side the lower Radar Facies 3 is more representative of 2D conditions and the upper Radar Facies 4 is more strongly 3D.

Radar Facies 5 – This represents all data near the crest of the dune (~100 m to the east of the peak to ~ 35 m west of the peak) (Fig. 13). It is characterized by long reflections (up to ~ 90 m on the east side and ~ 30 m on the west side) that originate near the peak of the dune and are truncated by shallower reflections, or the surface of the dune, as they approach the inflection point, or the location where the dune shallows out (Fig. 9). These reflections are taken to be mass wasting avalanche deposits on the slip face of the dune. The location of the active slip face appears to alternate frequently, since the surface profiles and subsurface

Fig. 12. (a) Collecting OSL sample from the large linear dune plinth (location in Fig. 4a). Sands were dry to 0.7 m. (b) Surface dune sand from near our OSL collection site. Grains are slightly coarse sand, ~0.5 mm. (c) Collecting OSL sample from interdune soils, finer-grained and more cohesive than dune sands. (d) Interdune surface west of our main study dune, mainly silt covered in sands and quartz cobbles of up to several cm. Pics from Jani Radebaugh.

Table 1
Optically Stimulated Luminescence Age (OSL) Information.

Sample num.	USU num.	Depth (m)	Num. of aliquots[1]	Dose Rate (Gy/ka)	D_E[2] ± 2σ (Gy)	OD[3] (%)	OSL age ± 2σ (ka)
Namibia Roter Kamm 1	USU-1623	1	22 (42)	2.34 ± 0.13	102.3 ± 18.2	38.2 ± 6.7	**43.7 ± 8.4**
Namib 2	USU-1624	1	18 (44)	2.09 ± 0.11	0.26 ± 0.38 [4]	108.5 ± 24.4	**0.12 ± 0.18**
Namib Interdune 1	USU-1625	0.61	19 (41)	2.53 ± 0.14	129.2 ± 17.4	25.2 ± 5.4	**51.0 ± 7.8**

[1] Age analysis using the single-aliquot regenerative-dose procedure of Murray and Wintle (2000) on 1–2 mm small-aliquots of quartz sand. Number of aliquots used in age calculation and number of aliquots analyzed in parentheses.
[2] Equivalent dose (De) calculated using the Central Age Model (CAM) of Galbraith and Roberts (2012), except where noted otherwise. Age model software written by Sebastién Huot (ISGS).
[3] Overdispersion (OD) represents variance in D_E data beyond measurement uncertainties, OD greater than 20% may indicate significant scatter due to depositional or post-depositional processes.
[4] D_E calculated using the unlogged Minimum Age Model (MAM-UL) following Arnold et al. (2009).

Table 2
Dose rate information.

Sample num.	USU num.	Grain size (μm)	H_2O[1] (%)	K (%)[2]	Rb (ppm) [2]	Th (ppm) [2]	U (ppm) [2]	Cosmic (Gy/ka)
Namibia Roter Kamm 1	USU-1623	150–250	0.14	1.60 ± 0.04	71.7 ± 2.9	6.6 ± 0.6	0.8 ± 0.1	0.19 ± 0.02
Namib 2	USU-1624	150–250	0.02	1.39 ± 0.03	67.7 ± 2.7	5.4 ± 0.5	1.0 ± 0.1	0.17 ± 0.02
Namib Interdune 1	USU-1625	125–250	0.28	1.22 ± 0.03	54.2 ± 2.2	11.0 ± 0.1	1.9 ± 0.1	0.19 ± 0.02

[1] In-situ gravimetric water content, assumed 3 ± 3% for moisture content to represent burial history for all samples.
[2] Radioelemental concentrations determined by ALS Chemex using ICP-MS and ICP-AES techniques, dose rate is derived from concentrations by conversion factors from Guérin et al., 2011.

GPR profiles are similar on either side. This is likely a result of seasonal changes in dominant winds, discussed in detail below.

Area 1 – This area is located at the inflection points on both sides of the dune (Fig. 13), where Radar Facies 5 is seen to be interfingering with the other facies (Fig. 13). In this area we can see the variation in the dominance of each process (superimposed dunes and primary crest).

Superposition Surface – This boundary occurs between Radar Facies 1 and 2 on the west flank of the dune and Radar Facies 3 and 4 on the east flank (Fig. 13), at about 1–3 m depth. This boundary truncates underlying reflections, which onlap or downlap against the boundary (Fig. 7a and b). The boundary is continuous from where it begins near the inflection point on both sides of the dune until it meets the interdune surface on the west side of the dune and until the end of the data on the east side (the track did not continue all the way to the interdune on the east side).

The Superposition Surface is significant in that it seems to indicate a change in depositional style, and therefore primary wind regime, over long enough time periods to allow several meters worth of deposition.

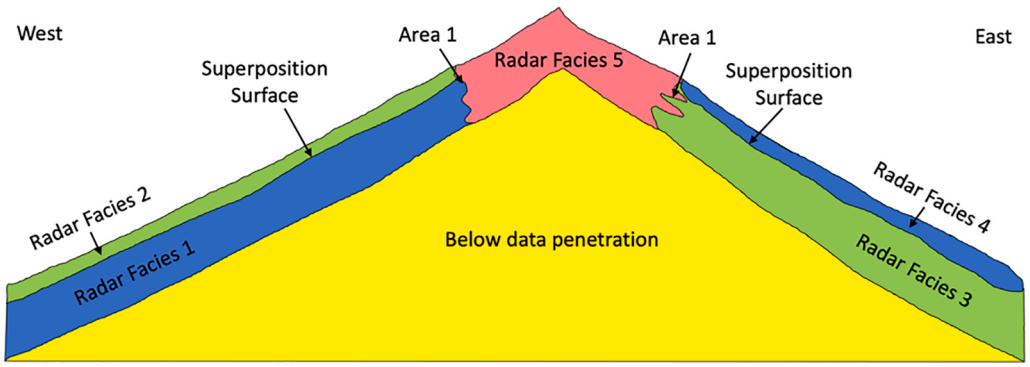

Fig. 13. Cartoon of the interpreted radar facies. Note that the area of interest encompasses nearly the entire dune and is thus greatly exaggerated to be able to show the relationships between interpreted features. Discussions in the text reveal morphological similarities between Radar Facies 1 and 4 and Radar Facies 2 and 3, shown here in similar tones.

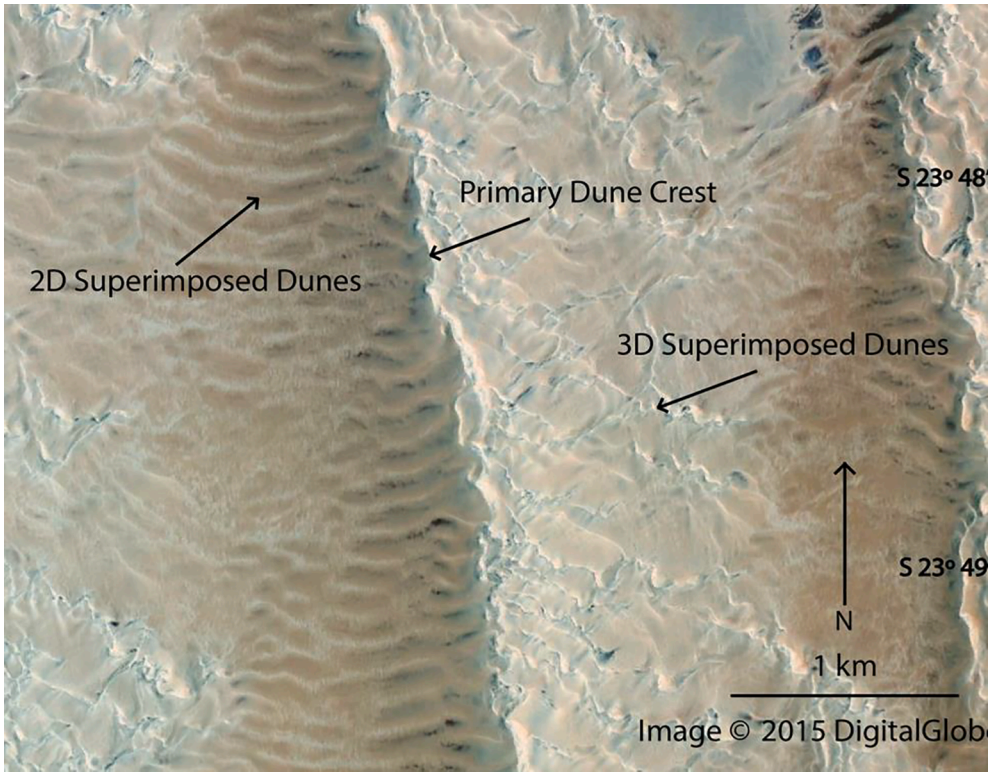

Fig. 14. Dunes just southwest of our study area, showing the placement of modern 2D and 3D dunes in the Namib with respect to the main dune crestline. Labeled on the right of the main dune crestline are 3D superimposed dunes similar to what we expect to have deposited the TCS patterns in Radar Facies 1 and 4 of Fig. 13. The 2D superimposed dunes on the left of the main dune crestline are traversing the crest to the north and are similar to what we expect to have deposited Radar Facies 2 and 3 of Fig. 13. Base image from Google Earth.

This boundary relates to changes over time in the superimposed dunes, which have strong and consistent characteristics across much of the Namib Sand Sea. The superimposed dunes on the west side of the primary dune display a 2D waveform, have relatively straight crests oriented more or less perpendicular to the main dune crest, and they extend from the inflection point to the interdune surface. On the east side of the primary dune, the superimposed dunes display a 3D waveform, are arcuate, and extend from the inflection point down the dune toward the interdune surface. They have a long axis that is oriented oblique to the primary dune crest, toward the southeast (Fig. 13).

The difference in the shapes of the superimposed dunes on each side of the primary dune suggests that slightly different wind conditions and sand transport styles are responsible for sand movement on each side of the primary dune. Winds and sand transport appear to be effectively to the north on the west side of the dune, creating 2D bedforms, while on the east side, winds appear to be more complex, causing eastward elongation and sinuosity in the generally northward-transporting, 3D dunes. Furthermore, the depositional patterns observed by GPR at depth on either side of the primary dune crest are opposite from what they are at the surface, indicating a reversal in these wind regimes and depositional styles over time. This may be a result of wind deflection as a result of the dune itself coupled with dominant seasonal winds, and is discussed more below.

Crossing dune GPR interpretation

The GPR data for the crossing dune examine a shallower depth than the data for the large linear dune and are more readily interpretable. Reflections occur with dips primarily to the east-northeast on the dune crestline, or down the dune long axis, and primarily to the north-northwest on the cross lines, or trending between parallel and perpendicular to the dune long axis (Fig. 11a, b). We interpret these dipping reflections to be depositional foresets, with the dip indicating the direction of sand transport. The crestline and dipline tracks indicate

slightly different transport directions, but when viewed in combination, they reveal a sum total in the sand transport direction at the time of formation to the NE.

The GPR data of the crossing dune reveal that the dune overall has 3D characteristics and that sand transport is longitudinal to oblique northward to the orientation of the crest. Crossing dunes are found throughout the Namib Sand Sea, though they are longer and more pronounced in the areas around Tsondab Vlei, a dry river valley (now undergoing some dune recovery since the recession of the Tsondab River in the Quaternary; e.g. Teller et al., 1990). In this region, there is less sand, and the distribution of large, linear dunes is more sparse. It is possible that large, linear dunes need more time to fully recover in the vlei, and that modern conditions are better for the formation of crossing dunes. If the crossing dunes form by elongation, the wind regime east of this location is favorable for it; there is a strong component parallel to the crossing forms. This is discussed below.

Change in wind in the Namib

The GPR data for our main study dune, coupled with satellite observations of the regional dune morphology, are best explained by a change in dominant wind conditions over the recent past, based on the depth of observations of this change at 1–3 m. Similar depths yielded OSL ages of a few hundred years on an active portion of a dune on the margin of the sand sea north of our study area, compared with over 5700 years of stability in the middle portion of a dune at great depths (Bristow et al., 2007). Previous studies have noted the dominance of winds to the north-northeast, with winds to the southwest in winter (Breed and Grow, 1979; Lancaster, 1985; Lancaster, 1989; Livingstone, 1989). These winds are postulated to have elongated the large, linear dunes in the Namib through down-axis sedimentation, mainly toward the north (Bristow et al., 2000; Tsoar et al., 2004; Livingstone, 2003; Bullard et al., 2011). These two main wind directions, to the north-northeast and to the southwest, have current relative sand flux potentials, or the ability to move sand, of 60–80% and 15–20%, respectively (Lancaster, 1985), and result in down-axis transport because of their deflection by the dune crest and their wide-angle bimodality (Parteli et al., 2009).

Time-averaged winds in the Namib Sand Sea have also been obtained by integrating surface wind station and satellite observational data with models for atmospheric circulation, producing the ERA-Interim Project reanalysis model (Dee et al., 2001; Dee et al., 2011). This has significantly improved temporal and spatial resolution over other models (80–90 km at this latitude). Fig. 15 shows modeled wind speeds and directions (colored roses) for regions near our study area, averaged across the year and since 1979. Note that roses extend in the direction wind is flowing. From these values, using sediment flux laws on a flat sand bed from Ungar and Haff (1987) and Lettau (1978) and assuming a threshold wind velocity for sand movement of 4.4 + -1 m/s at 10 m height, resultant sand fluxes were calculated and are shown as green roses (Fig. 15). The dominance of winds to the north-northeast is evident in these wind roses, as is the presence of minor secondary winds blowing towards the southwest (Fig. 15). The calculated sand flux from these wind directions is mainly to the north-northeast (roses 13 in Fig. 15). This broadly aligns with the orientations of the large linear dune long axes and corroborates the model of linear dune elongation down-axis (Courrech du Pont et al., 2014; Lucas et al., 2014; Lucas et al., 2015). Note, however, there is a southwesterly component to the sand

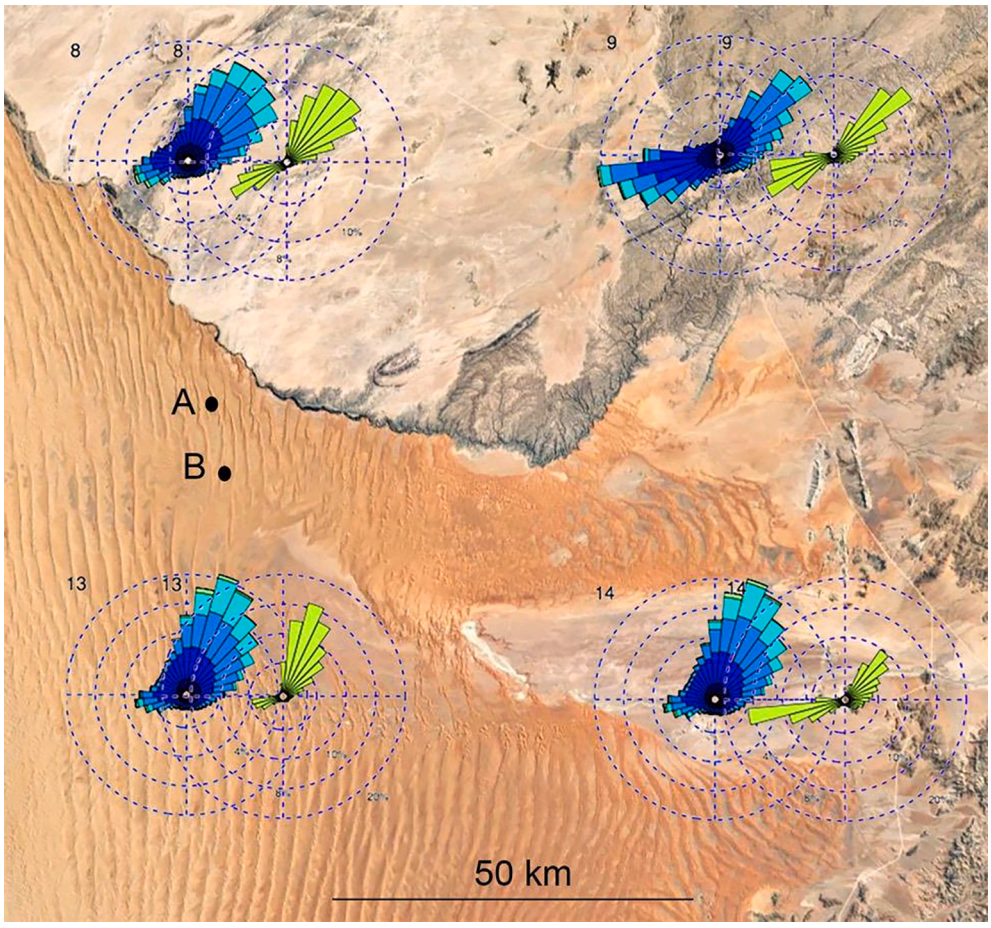

Fig. 15. ERA-Interim model wind direction and magnitude for the Namib Sand Sea (colored roses), maximum values here ~ 5 m/s. Roses extend in direction of wind flow. Green roses show sediment flux magnitude and direction. Numbers at upper left of roses are ERA-Interim model regional identifiers.

transport, which may act to preserve sands within the sand sea.

During current summer conditions, we postulate that winds to the north-northeast carry sands along the west side of the dune in a transverse dune-like, 2D dune flux scenario (Rubin and Hunter, 1987; Fig. 14). This is also termed the bed instability mode model for sand transport (Courrech du Pont et al., 2014). The southwest-directed winds on the east side of the dune may cause the complexity seen in the flanking, 3D dunes (Tsoar, 1983; Bristow et al., 2000; Fig. 12). The combination of these winds with the northward winds cause the 3D secondary dunes to elongate away from the main, large linear dune crest along the secondary dune crest axis, termed the fingering mode of dune propagation (Courrech du Pont et al., 2014; Lucas et al., 2015). In this model of sand transport, sand transport and elongation occurs down the secondary dune (as opposed to transverse to it). These dunes are larger than the 2D transverse dunes, and deeper scouring as a result of their passage may have caused more recent overturn of sands at 2–4 m depth, ~9 ka, in a sample dune in the southern Namib (Bubenzer et al., 2007). In contrast, overturn ages of sands on the west side of an adjacent dune at the same depths revealed ages of up to 22 ka. Perhaps sand movement on the west is extremely shallow from the gentler passage of the 2D transverse dunes.

Comparison of high-resolution images of the region from 2010 and 2015 reveals there was total northward movement on the western 2D dunes, north-northeastward movement on the eastern 3D dunes and alternating west-east and northward movement on the main linear dune crest. Maximum values for this movement (comparing dune sand with locations of bushes present in both images) were 15–25 m in 5 years, and nearly all of this movement was on active, non-vegetated crests of the main and flanking dunes. No lateral movement occurred on the large dune margin. This is similar to rates reported by Livingstone (1993; 2003).

If the current prevailing wind condition were that the dominant wind was the winter wind, to the southwest, this flow, and the resultant features, would be opposed, almost as a mirror image of the dune surface structure seen in Fig. 14. Perhaps in times of a stronger, or longer, winter climate, this would become the dominant wind pattern and the dune features would switch, leading to 3D forms on the west and 2D forms on the east. This wind condition could be responsible for the deeper GPR signatures observed. The timeframe for this change could be on the order of hundreds of years, based on OSL dates near the process boundary obtained by Bristow et al. (2007).

The current winds as seen in the ERA-Interim wind model may also help explain the presence of the crossing dunes. Note that the dominant wind north of our study area is directed toward the ENE, almost aligning with the orientations of the crossing dunes (sediment flux directions in roses 8, 9 in Fig. 15). These winds result in a sediment flux to the NE of the axis of the crossing dunes, similar to what was observed in the GPR data. Movement on the crossing dunes over the same 2010–2015 time frame as observed in high-resolution images was restricted to minor, active portions of the crestline.

Additional information on winds comes from the Paleoclimate Modelling Intercomparison Project (PMIP), which examines the last 20 ka through Global Circulation Models, covering the Last Glacial Maximum and potential dune-forming time frame in the Namib (Lancaster, 1989). Predicted winds and sediment fluxes from these models are similar to those for the ERA-Interim wind model results for this region of the Namib, including the major and minor wind directions and northeastward transport near the crossing dunes. This means that, according to the PMIP and ERA-Interim models, wind conditions have not varied drastically over the past 20 ka. Perhaps the differences in wind conditions on the dune flanks leading to changes in 2D or 3D forms are relatively small compared to the inputs to these GCMs and are not manifest as changes to the broad-scale wind pattern. This reinforces the predicted long-term stability of the large, linear dunes in the Namib Sand Sea (Lancaster, 1989). Indeed, transport of sand below several meters depth seems to have tapered off around this time, as evidenced by sand exposure ages between 22 ka and 9 ka at up to 4 m depth in the southern Namib Sand Sea (Bubenzer et al., 2007). The existence of sand transport conditions locally subparallel to the crossing dunes as far back as 20 ka indicates these forms possibly co-evolved with the large, linear dunes. However, why both forms exist alongside each other and neither has absorbed the other is not understood. Perhaps the unique conditions of nearly oppositely directed seasonal winds are unique to the Namib, and cause, throughout their history, contortions to the dune crest, the presence of complex flanking features and the existence of the significant crossing forms. Alternatively, these smaller superimposed dunes may reflect recent winds and available sediment conditions, while the older forms were built during different conditions, as was determined through pattern analysis of West African superimposed forms (Ewing et al., 2006).

Implications for linear dune formation on Titan

Large sand seas cover the equatorial regions of Saturn's moon Titan (Lorenz et al., 2006; Radebaugh et al., 2008; Radebaugh, 2013; Rodriguez et al., 2014). The linear dunes have morphologies similar to those of Earth's large deserts in size, spacing and behavior around obstacles, making the Namib Sand Sea a good analogue for the sand seas of Titan (Fig. 16; Lorenz et al., 2006; Lorenz and Radebaugh, 2016). The orientations of the dunes on Titan and their interactions with topographic obstacles have been used to determine sand flux directions, which are assumed to be dominantly down-axis (Radebaugh et al., 2008; Lucas et al., 2015), and broadly and globally toward the east (Radebaugh et al., 2008; Lorenz and Radebaugh, 2009). Applying the understanding that sand flux directions are related to winds, with new models recognizing a dominant wind just off-axis, with other secondary winds, the general direction of winds at the surface capable of carrying sands has been determined to be broadly from the west to the east (Lucas et al., 2015). This is possible on Titan during the change of seasons (Tokano, 2010) or during strong, equinoctial storms (Charnay et al., 2015).

What appears to be missing from Titan's dune fields compared with the Namib are the large-scale, flanking or crossing dunes, the largest of which should be visible at Cassini SAR resolutions (Fig. 16; Savage et al., 2014). Perhaps the lack of these features indicates that the complex wind regime of the Namib is missing on Titan. Instead, there may be comparatively simple wind conditions, or stability and equilibrium over long timescales. Dunes on Titan may be in an equilibrium state with the current atmospheric and wind conditions (Savage et al., 2014) and given the size and construction times of large linear dunes, these conditions could have prevailed with similar morphologies for a long time (Ewing et al., 2015).

However, even the most simple large linear dunes on Earth have secondary forms, commonly the 2D transverse dunes discussed in this work. These smaller forms would not be visible at Cassini SAR resolutions (Savage et al., 2014). Given that the dunes are expected to be active (Barnes et al., 2008), high-resolution imagery, such as from the Dragonfly rotorcraft lander dune region mission (Lorenz et al., 2017), will likely reveal secondary and flanking forms, as well as complex and changing crestlines, on the large linear/longitudinal dunes of Titan.

Conclusions

We obtained high-resolution, high-quality GPR data for linear dunes of the Namib Sand Sea, on regions that have not been imaged before, and their detail allows for a more intensive level of interpretation of the evolution of large, complex, linear dunes, and their relationship to variations in wind conditions between seasons, and through time. These images are the highest resolution images of the subsurface of Namib dunes yet available. Their detail allows for a more intensive level of interpretation and relationship to variations in wind conditions. Though it is a single trace, this study has value in revealing several different sedimentary zones bounded by a relatively straight, erosional

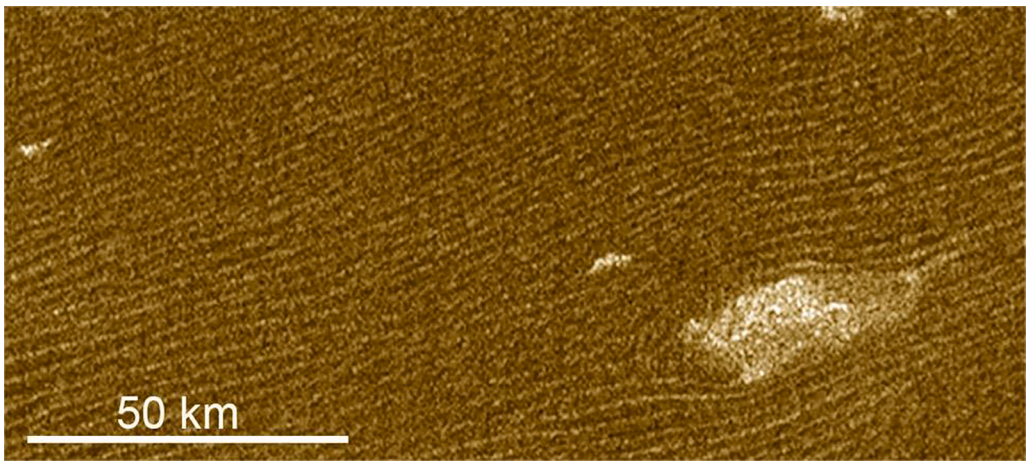

Fig. 16. Dunes in Titan's Belet Sand Sea, located ~ 250 W, 8 S. Image is Synthetic Aperture RADAR, so dark materials represent the smooth dunes, while bright materials are rough interdunes or topographic obstacles. Note the overall straight pattern to the dune crests. North is up. Image from the T8 flyby of Titan by Cassini, Feb. 2007, resolution ~ 300 m.

superposition surface. The different superimposed dune morphologies (2D and 3D) on opposite flanks of the primary large linear dune indicate a difference in flow regime from one side of the dune to the other. 2D dunes on the western side indicate northward (summer) winds and sand transport, while 3D dunes on the east indicate a combination of northward and SW (winter) directed winds and sand transport. We show that opposing dune flanks display an opposite stratigraphic succession, indicating a change in flow energy and/or direction of wind from below the superposition surface to above the boundary. This change in energy is likely a regional forcing mechanism, as its modern pattern is observable over great distances within the Namib Sand Sea. We speculate that the change in energy is oscillatory, perhaps in changing the dominant sand-transporting winds from summer northeast winds to winter southwest winds, and may be involved in the down-axis growth and lateral stability of large, complex, linear/longitudinal dunes on Earth. Further research may aid in determining whether the stratigraphic stacking pattern continues deeper into the dune and if it is found throughout the sand sea and in other sand seas.

Secondary dune forms found flanking the main linear dune are common here as on other large, linear dunes. In particular, the 2D transverse dune pattern on the flanks and sometimes in the interdune areas of large linear dunes is found in many sand seas. These forms reveal modern details of prevailing winds and sediment transport – in this case, they reveal current northward transport of sand on the western flanks. The 3D elongated secondary dune pattern on the eastern side likely arises from the combination of the SW and northern winds. Both patterns should be studied in more depth, ideally with a 3D GPR survey.

The unique crossing dune pattern we observed that likely results from sand transport down minor linear dunes away from the main linear dunes emphasizes the northward and down-axis transport of sand on linear dunes and the dependence of this transport on wind direction. The crossing dunes appear to have migrated obliquely to the main dune, reflecting modern and paleo winds estimated as far back as 20 ka. This indicates that these features may be relatively stable. The features may also indicate that some wind conditions, such as the complex one in the Namib, allow for the co-formation of large linear dunes with crossing and flanking features, or these winds are stable for crossing dune formation, while prior conditions facilitated large dune growth. The lack of crossing dunes at large scales on Titan's dunes reveals an overall stable, and perhaps simple, wind regime over time.

Field studies in sand seas on Earth, in particular the introduction of the subsurface data, reveal changes that occur in large linear/longitudinal dunes over time. The overall formative histories and knowledge of wind regimes on Earth help us develop models for dune requirements that we can apply to Titan. Conversely, on Titan, the relative climatic stability and lack of intervening oceans, topography or vegetation allows for possibly unrestrained growth of the dunes and sand seas, which, when observed, feeds back into our understanding of these important eolian landforms on Earth.

Declaration of Competing Interest

The authors declare that they have no known competing financial interests or personal relationships that could have appeared to influence the work reported in this paper.

Acknowledgements

We would like to thank the staff and general support at Gobabeb, especially Theo Wassenaar and Titus Shuuya, without whom our field work would have been impossible. We would also like to thank the Namibian government for allowing us to do field work in the sand sea. We thank two anonymous reviewers for their detailed and extremely helpful reviews. Field work for this study was supported by the College of Physical and Mathematical Sciences and by generous donations to the college. Data processing and visualization were made possible by software grants from the Landmark (Halliburton) University Grant Program and from the IHS Kingdom Educational Grant Program. S.R. acknowledges financial support from the UnivEarthS LabEx program of Sorbonne Paris Cite (ANR-10-LABX-0023 and ANR-11-IDEX-0005-02), the French National Research Agency (ANR-12-BS05-001-3/EXO-DUNES) and the Institut Universtaire de France.

References

Andreotti, B., Fourriere, A., Ould-Kaddour, F., Murray, B., Caudin, P., 2009. Giant aeolian dune size determined by the average depth of the atmospheric boundary layer. Nature 457, 1120–1123.

Arnold, K., 2014. Sand Sea Areas and Sediment Volumes on Titan from Dune Parameters. Brigham Young University, Thesis.

Arnold, L.J., Roberts, R.G., Galbraith, R.F., DeLong, S.B., 2009. A revised burial dose estimation procedure for optical dating of young and modern-age sediments. Quat. Geochronol. 4, 306–325.

Barnes, J.W., Brown, R.H., Soderblom, L., Sotin, C., Le Mouelic, S., Rodriguez, S., Jaumann, R., Beyer, R.A., Clark, R., Nicholson, P., 2008. Spectroscopy, morphometry, and photoclinometry of Titan's dunefields from Cassini/VIMS. Icarus 195, 400–414.

Breed, C.S., Grow, T., 1979. Morphology and distribution of dunes in sand seas observed by remote sensing. In: E. D. McKee, (Ed.), A Study of Global Sand Seas, pp. 253-302.

Bristow, C.S., 2009. Ground penetrating radar in aeolian dune sands, in: Ground penetrating radar: theory and applications, pp. 273-297.

Bristow, C.S., Bailey, S.D., Lancaster, N., 2000. Sedimentary structure of linear sand dunes. Nature 406, 56–59.

Bristow, C.S., Lancaster, N., Duller, G.A.T., 2005. Combining ground-penetrating radar (GPR) surveys and optical dating to determine dune migration in Namibia. Geol. Soc. [Lond.] J. 162, 315–321. https://doi.org/10.1144/0016-764903-120.
Bristow, C.S., Duller, G.A.T., Lancaster, N., 2007. Age and dynamics of linear dunes in the Namib Desert. Geology 35, 555–558.
Bubenzer, O., Hilgers, A., Riemer, H., 2007. Luminescence dating and archaeology of Holocene fluvio-lacustrine sediments of Abu Tartur, Eastern Sahara. Quat. Geochronol. 2, 314–321.
Bullard, J.E., White, K., Livingstone, I., 2011. Morphometric analysis of aeolian bedforms in the Namib Sand Sea using ASTER data. Earth Surf. Proc. Land. 36 (11), 1534–1549.
Charnay, B., Barth, E., Rafkin, S., Narteau, C., Lebonnois, S., Rodriguez, S., Du Pont, S.C., Lucas, A., 2015. Methane storms as a driver of Titan's dune orientation. Nat. Geosci. 8 (5), 362.
Cooke, R.U., A. Warren 1973. *Geomorphology in deserts.* Univ of California Press.
Courrech du Pont, S., Morphodynamique des dunes. Comptes Rendus Physique 16, 118-138.
Courrech du Pont, S., Narteau, C., Gao, X., 2014. Two modes for dune orientation. Geology 42, 743–746.
Courrech du Pont, S., 2015. Dune morphodynamics. Comptes Rendus Physique 16 (1), 118–138.
Dee D.P., 35 others, 2001. The ERA-interim reanalysis: configuration and performance of the data assimilation system. Q. J. R. Meteorol. Soc. 137, 553–597.
Dee, D.P., Uppala, S.M., Simmons, A.J., Berrisford, P., Poli, P., Kobayashi, S., Andrae, U., Balmaseda, M.A., Balsamo, G., Bauer, D.P., Bechtold, P., 2011. The ERA-Interim reanalysis: Configuration and performance of the data assimilation system. Q. J. R. Meteorolog. Soc. 137, 553–597.
Dong, Z., Wei, Z., Qian, G., Zhang, Z., Luo, W., Hu, G., 2010. "Raked" linear dunes in the Kumtagh Desert, China. Geomorphology 123, 122–128.
Ewing, R.C., Kocurek, G., Lake, L.W., 2006. Pattern analysis of dune-field parameters. Earth Surf. Process. Landforms: J. British Geomorphol. Res. Group 31, 1176–1191.
Ewing, R.C., Hayes, A.G., Lucas, A., 2015. Sand dune patterns on Titan controlled by long-term climate cycles. Nature. https://doi.org/10.1038/ngeo2323.
Fryberger S.G., 1979, Dune forms and wind regime. In: A study of global sand seas (Ed. By E. D. McKee) professional paper U. S. Geological Survey, 1052 p. 137-170.
Fryberger, S.G., Goudie, A.S., 1981. Arid geomorphology. Progr. Phys. Geogr. 5, 420–428.
Galbraith, R.F., Roberts, R.G., 2012. Statistical aspects of equivalent dose and error calculation and display in OSL dating: An Overview and some recommendations. Quaternary Geochronology 11, 1–27.
Garzanti, E., Ando, S., Vezzoli, G., Lustrino, M., Boni, M., Vermeesch, P., 2012. Petrology of the Namib Sand Sea: Long-distance transport and compositional variability in the wind-displaced Orange Delta. Earth-Sci. Rev. 112, 173–189.
Gawthorpe, R.L., Collier, R.L., Alexander, J., Bridge, J.S., Leeder, M.R., 1993. Ground penetrating radar: application to sandbody geometry and heterogeneity studies. Geol. Soc. Lond. Spec. Publ. 73, 421–432.
Guérin, G., Mercier, N., Adamiec, G., 2011. Dose-rate conversion factors: update. Ancient Tl 29 (1), 5–8.
Havholm, K.G., Kocurek, G., 1994. Factors controlling aeolian sequence stratigraphy: clues from super bounding surface features in the Middle Jurassic Page Sandstone. Sedimentology 41 (5), 913–934.
Holm, D.A., 1960. Desert geomorphology in the Arabian Peninsula. Science 132 (3437), 1369–1379.
Huggenberger, P., 1993. Radar facies: recognition of facies patterns and heterogeneities within Pleistocene Rhine gravels, NE Switzerland. Geol. Soc. Lond. Spec. Publ. 75, 163–176.
Kocurek, G., 1981. Significance of interdune deposits and bounding surfaces in aeolian dune sands. Sedimentology 28, 753–780.
Kocurek G. and Havholm K. 1993. Eolian sequence stratigraphy - a conceptual framework. In: Siliciclastic Sequence Stratigraphy (Ed. by P. Weimer & H. Posamentier). American Association of Petroleum Geologists Memoir 58, 393-409.
Kocurek, G., Lancaster, N., Carr, M., Frank, A., 1999. Tertiary Tsondab Sandstone Formation: Preliminary bedform reconstruction and comparison to modern Namib Sand Sea dunes. J. Afr. Earth Sc. 29 (4), 629–642.
Lancaster, N., 1982. Linear dunes. Prog. Phys. Geogr. 6, 476–504.
Lancaster, N., 1985. Winds and Sand Movements in the Namib Sand Sea. Earth Surf. Proc. Land. 10, 607–619.
Lancaster, N., 1989. The Namib Sand Sea: Dune forms, processes, and sediments: Rotterdam. Balkema, A.A, p. 200.
Lancaster, N., 1995, Geomorphology of desert dunes: London, Routledge, 290 p.
Lettau, K., 1978. Experimental and micrometeorological field studies of dune migration. Exploring in the World's driest climate 110–147.
Livingstone, I., 1989. Monitoring surface change on a Namib linear dune. Earth Surf. Proc. Land. 14, 317–332.
Livingstone, I., 1993. A decade of surface change on a Namib linear dune. Earth Surf. Proc. Land. 18, 661–664.
Livingstone, I., 2003. A twenty-one-year record of surface change on a Namib linear dune. Earth Surf. Proc. Land. 28, 1025–1032.
Livingstone, I., Wiggs, G.F.S., Weaver, C.M., 2007. Geomorphology of desert sand dunes: a review of recent progress. Earth-Sci. Rev. 80, 239–257.
Livingstone, I., Bristow, C., Bryant, R.G., Bullard, J., White, K., Wiggs, G.F., Baas, A.C., Bateman, M.D., Thomas, D.S., 2010. The Namib Sand Sea digital database of aeolian dunes and key forcing variables. Aeolian Res. 2, 93–104.
Lorenz, R.D., Radebaugh, J., 2009. The Global Pattern of Titan's Dunes: Radar Survey from the Cassini Prime Mission. Geophys. Res. Lett. 36, L03202. https://doi.org/10.1029/2008GL036850.
Lorenz, R.D., Zimbleman, J.R., 2014. Dune Worlds: How Windblown Sand Shapes Planetary Landscapes. Springer-Praxis, Chichester, UK, p. 308.
Lorenz, R.D., Radebaugh, J., 2016. To Titan, via Namibia. Commun. Geol. Survey Namibia 17, 1–15.
Lorenz, R.D., Wall, S., Radebaugh, J., Boubin, G., Reffet, E., Janssen, M., Stofan, E., Lopes, R., Kirk, R., Elachi, C., Lunine, J., Paganelli, F., Soderblom, L., Wood, C., Wye, L., Zebker, H., Anderson, Y., Ostro, S., Allison, M., Boehmer, R., Callahan, P., Encrenaz, P., Ori, G.G., Francescetti, G., Gim, Y., Hamilton, G., Hensley, S., Johnson, W., Kelleher, K., Mitchell, K., Muhleman, D., Picardi, G., Posa, F., Roth, L., Seu, R., Shaffer, S., Stiles, B., Vetrella, S., Flamini, E., West, R., 2006. The Sand Seas of Titan: Cassini RADAR observations of Longitudinal Dunes. Science 312, 724–727.
Lorenz, R.D., E.P. Turtle, J.W. Barnes, M.G. Trainer, D.S. Adams, K.E. Hibbard, C.Z. Sheldon, K. Zacny, P.N. Peplowski, D.J. Lawrence, M.A. Ravine, T.G. McGee, K.S. Sotzen, S.M. MacKenzie, J.W. Langelaan, S. Schmitz, L.S. Wolfarth, and P.D. Bedini 2017. Dragonfly: A Rotorcraft Lander Concept for Scientific Exploration at Titan. Johns Hopkins APL Technical Digest, www.jhuapl.edu/techdigest.
Lucas, A., Rodriguez, S., Narteau, C., Charnay, B., Courrech du Pont, S., Tokano, T., Garcia, A., Thiriet, M., Hayes, A.G., Lorenz, R.D., Aharonson, O., 2014. Growth Mechanisms and Dune Orientation on Titan. Geophys. Res. Lett. https://doi.org/10.1002/2014GL060971.
Lucas, A., Narteau, C., Rodriguez, S., Rozier, O., Callot, Y., Garcia, A., Courrechdu Pont, S., 2015. Sediment flux from the morphodynamics of elongating linear dunes. Geology 43, 1027–1030.
Mainguet, M., Callot, Y., 1978. L'erg de Fachi-Bilma (Tchad-Niger). Memoires et Documents CNRS 18, 178.
McKee E. D., 1979, a study of global sand seas: professional paper U. S. Geological Survey, 1052.
McKee E. D., 1982, sedimentary structures in dunes of the Namib Desert, South West Africa: special paper Geological Society of America, 188.
Munyikwa, K., 2005. The role of dune morphogenetic history in the interpretation of linear dune luminescence chronologies: A review of linear dune dynamics. Prog. In Phys. Geog. 29, 317–336.
Murray, A.S., Wintle, A.G., 2000. Luminescence dating of quartz using an improved single aliquot regenerative-dose protocol. Radiat. Measur. 32, 57-73.
Murray, A.S., Wintle, A.G., 2003. The single aliquot regenerative dose protocol: potential for improvements in reliability. Radiat. Meas. 37, 377–381.
Parteli, E., Duran, O., Tsoar, H., Schwammle, V., Herrmann, H., 2009. Dune formation under bimodal winds. Proc. Natl Acad. Sci. 1106, 22085–22089.
Radebaugh, J., 2013. Dunes on Saturn's moon Titan as revealed by the Cassini Mission. Aeolian Res. 11, 23–41.
Radebaugh, J., R. Lorenz, J. Lunine, S. Wall, G. Boubin, E. Reffet, R. Kirk, R. Lopes, E. Stofan, L. Soderblom, M. Allison, M. Janssen, P. Paillou, P. Callahan and the Cassini Radar Team 2008. Dunes on Titan observed by Cassini Radar. Icarus 194, 690-703, doi:10.1016/j.icarus.2007.10.015.
Reffet, E., Courrech du Pont, S., Hersen, P., Douady, S., 2010. Formation and Stability of transverse and longitudinal sand dunes. Geology 38, 491–494.
Rodriguez, S., A. Garcia, A. Lucas, T. Appéré, A. Le Gall, E. Reffet, L. Le Corre, S. Le Mouélic, T. Cornet, S. Courrech du Pont, C. Narteau, O. Bourgeois, J. Radebaugh, K. Arnold, J.W. Barnes, C. Sotin, R.H. Brown, R.D. Lorenz, E.P. Turtle 2014. Global mapping and characterization of Titan's dune fields with Cassini: correlation between RADAR and VIMS.
Rubin, D., Hunter, R., 1987. Bedform alignment in directionally varying flows. Science 237, 276–278.
Rubin, D.M., Ikeda, H., 1990. Flume experiments on the alignment of transverse, oblique and longitudinal dunes in directionally varying flows. Sedimentology 37, 673–684.
Savage, C.J., Radebaugh, J., Christiansen, E.H., Lorenz, R.D., 2014. Implications of dune pattern analysis for Titan's surface history. Icarus 230, 80–190.
Singhvi, A.K., Porat, N., 2008. Impact of luminescence dating on gemorphological and palaeoclimate research in drylands. Boreas 36, 536–558.
Stone, A.E.C., Thomas, D.S.G., Viles, H.A., 2010. Late Quaternary palaeohydrological changes in the northern Namib Sand Sea: new chronologies using OSL dating of interdigitated aeolian and water-lain interdune deposits. Palaeogeogr. Palaeoclimatol. Palaeoecol. 288, 35–53.
Stone, A.E., Bateman, M.D., Thomas, D.S., 2015. Rapid age assessment in the Namib Sand Sea using a portable luminescence reader. Quat. Geochronol. 30, 134–140.
Teller, J.T., Rutter, N., Lancaster, N., 1990. Sedimentology and paleohydrology of Late Quaternary lake deposits in the northern Namib Sand Sea, Namibia. Quat. Sci. Rev. 9, 343–364.
Tokano, T., 2010. Relevance of fast westerlies at equinox for the eastward elongation of Titan's dunes. Aeolian Res. 2, 113–127.
Topp, G.C., Zebchuk, W.D., Dumanski, J., 1980. The variation of in situ measured soil water properties within soil map units. Can. J. Soil Sci. 60, 497–509.
Tsoar, H., 1982. Internal structure and surface geometry of longitudinal (seif) dunes. J. Sedim. Perol. 52 (3), 0823–0831.
Tsoar, H., 1983. Dynamic processes acting on a longitudinal (seif) sand dune. Sedimentology 30, 567–578.
Tsoar, H.T., Blumberg, D.G., Stoler, Y., 2004. Elongation and Migration of sand dunes. Geomorphology 57, 293–302.
Ungar, J.E., Haff, P.K., 1987. Steady state saltation in air. Sedimentology 34 (2), 289–299.
Van Dam, R.L., Schlager, W., 2000. Identifying causes of ground-penetrating radar reflections using time-domain reflectometry and sedimentological analyses. Sedimentology 47, 435–449.
Vermeesch, P., Fenton, C. R., Kober, F., Wiggs, G. F. S., Bristow, C. S., Xu, S., 2010, Sand residence times of one million years in the namib sand sea from cosmogenic nuclides, Nat. Geosci. 3, 862-865.

Warren, A. 1988. The dunes of the Wahiba Sands. In, R.W. Dutton, ed., Scientific Results of the Royal Geographical Society's Oman Wahiba Sands Project 1985-1987, 131-160, Journal of Oman Studies, Special Report 3, Muscat, Oman.
Wilson, I.G., 1972. Aeolian bedforms—their development and origins. Sedimentology 19 (3–4), 173–210.
Wilson, I.G., 1973. Ergs. Sedim. Geol. 10, 77–106.
Wintle, A.G., Murray, A.S., 2006. A review of quartz optically stimulated luminescence characteristics and their relevance in single-aliquot regenerative protocols. Radiat. Meas. 41, 369–391.